Cancer Management and Research

Elevate Series

Open Access Full Text Article

ORIGINAL RESEARCH

The Actin Motor Protein Myosin 6 Contributes to Cell Migration and Expression of GIPC1 and Septins in Breast Cancer Cells

Magdalena Izdebska[1,*], Wioletta Arendt[1,*], Marta Hałas-Wiśniewska[1], Przemysław Zakrzewski[2], Robert Lenartowski[3,4], Marta Lenartowska[3,4]

[1]Department of Histology and Embryology, Faculty of Medicine, Nicolaus Copernicus University in Toruń, Collegium Medicum in Bydgoszcz, Bydgoszcz, Poland; [2]School of Cellular and Molecular Medicine, Faculty of Life Sciences, University of Bristol, University Walk, Bristol, UK; [3]Department of Cellular and Molecular Biology, Faculty of Biological and Veterinary Sciences, Nicolaus Copernicus University in Toruń, Toruń, Poland; [4]Centre for Modern Interdisciplinary Technologies, Nicolaus Copernicus University in Toruń, Toruń, Poland

*These authors contributed equally to this work

Correspondence: Magdalena Izdebska, Department of Histology and Embryology, Nicolaus Copernicus University in Toruń, Collegium Medicum in Bydgoszcz, 24 Karłowicza St, Bydgoszcz, 85-092, Poland, Tel +48 52 585 37 25, Email mizdebska@cm.umk.pl

Introduction: Breast cancer is highly metastatic. One protein that may participate in breast cancer cell migration is the actin motor protein myosin 6 (MYO6), which is likely regulated by the GIPC1 protein. Additionally, septins (SEPTs) appear to participate in breast cancer motility. Here, we investigated the effects of loss of MYO6 on cell morphology, migration, and expression of GIPC1, SEPT2, and SEPT7 in two breast cancer cell lines.

Material and Methods: The research material consisted of two breast cancer cell lines, MCF-7 and MDA-MB-231, in which the level of MYO6 was reduced and the effect of knockdown on the migration potential and the expression of GIPC1, SEPT2 and SEPT7 was determined. The levels of these proteins were also analyzed in silico.

Results: siRNA-mediated knock down of MYO6 altered the morphology of MCF-7 cells and reduced the expression of GIPC1 and SEPT7 in both MCF-7 and MDA-MB-231 cells. In in silico data, GIPC1, SEPT2, and SEPT7 were all overexpressed in breast cancer tissue samples from patients. Finally, MYO6 knock down impaired migration and adhesion in both MCF-7 and MDA-MB-231 cells.

Conclusion: Our study substantiates that downregulation of MYO6 diminishes the migratory abilities of breast cancer cell lines with varying invasiveness. Furthermore, we have demonstrated that decreased MYO6 protein leads to reduced expression of GIPC1, SEPT2, and SEPT7 in breast cancer cells. These findings contribute to a more comprehensive understanding of the pathways influencing breast cancer cell migration, a critical aspect of metastasis.

Keywords: MYO6, breast cancer, actin, migration, GIPC1, SEPT

Introduction

Breast cancer is often highly metastatic and invasive.[1] The movement of cancer cells from the primary tumor to distant sites involves a transition from an epithelial to a mesenchymal phenotype, requiring numerous molecular and morphological changes. One protein that appears to be important in cancer migration is the minus-end-directed actin motor protein myosin 6 (MYO6), which also participates in regulating cell migration in normal cells.[2]

Studies showed that MYO6 expression is upregulated in breast cancer samples, and its high expression correlates with poor prognosis.[3] Similarly, an analysis of TCGA colorectal cancer data revealed that MYO6 expression is significantly elevated in most colorectal cancer types compared to normal tissues. MYO6 overexpression contributes to increased cancer cell survival by inhibiting apoptosis.[4] Additionally, higher MYO6 expression correlates with the Gleason score, suggesting a role in prostate cancer progression.[5] However, not all cancers are characterized by increased levels of MYO6. Meng et al (2023) reported a significant decrease in

Received: 20 May 2024
Accepted: 22 September 2024
Published: 19 October 2024

MYO6 expression in clear cell renal cell carcinoma (ccRCC) compared to normal tissues, with ccRCC patients exhibiting high MYO6 levels having a poorer overall survival prognosis.[6]

An important regulator of MYO6 is GAIP interacting protein C-terminus 1 (GIPC1),[7,8] which binds to MYO6 via its C-terminal region. GIPC1 regulates various cellular processes such as proliferation, cell polarization, and cell migration. By interacting with integrins that indirectly link the extracellular matrix with actin filaments, GIPC influences actin cytoskeleton dynamics during cell migration.[9] Like MYO6, GIPC1 is overexpressed in breast cancer.[10,11] Moreover, Wu et al (2010) found that GIPC1 downregulation changes MDA-MB-231 breast cancer cells phenotype to less invasive.[12]

Another group of proteins that appear to participate in breast cancer cell motility are septins (SEPTs), a set of GTPases involved in organizing the actin and microtubule cytoskeletons.[13] SEPTs also associate with MYO6 and actin, and the DOCK7-Induced Septin displacement complex includes MYO6, Leucine-Rich repeats Calponin Homology domain, and Dedicator Of Cytokinesis 7.[14,15] SEPT2 and SEPT7 promote breast cancer cell migration and invasion.[13] Furthermore, SEPT2, SEPT8, SEPT9, and SEPT11 are overexpressed in Taxol-resistant breast cancer cells.[16] Kinoshita et al demonstrated the distribution of SEPTs along actin filaments in mammalian cells and showed that downregulation of SEPTs by siRNA disrupted actin filament bundle formation, leading to their self-assembling into cytoplasmic rings.[17] Furthermore, in studies using the SEPTs inhibitor Forchlorfenuron, Zhang et al (2016) observed an increase in the percentage of apoptotic cells, reduced proliferation, and colony formation in MCF-7 and MDA-MB-231 breast cancer cell lines. Additionally, downregulation of SEPTs in MDA-MB-231 cells significantly reduced migration and invasive abilities, leading to multinucleate accumulation and increased cell surface area.[13]

Together, the available data suggest that MYO6, GIPC1, and SEPTs may function together to regulate breast cancer motility. However, there is currently a lack of studies directly addressing this potential relationship. To address this gap, we examined the effects of MYO6 downregulation on the migratory behavior of breast cancer cells and its impact on these binding partners. The cell lines included in the study were MCF-7 and MDA-MB -231, which represent cells with low and high invasive properties, respectively.

Materials and Methods

Analysis of MYO6, GIPC1, SEPT2, and SEPT7 mRNA in TCGA and GTEx

Publicly available data from The Cancer Genome Atlas (TCGA) breast cancer cohort and The Genotype-Tissue Expression (GTEx) database were analyzed on the Xena platform (accessed on March 30th, 2024).[18] The dataset was normalized using the DESeq2 method, and 178 normal tissue samples were compared with 1099 tumor samples from patients.

Cell Culture

The breast cancer cell lines MDA-MB-231 and MCF-7 (American Type Culture Collection, Manassas, VA, USA) were cultivated 37 °C, 5% CO2, and 95% humidity. MCF-7 cells were grown in Eagle's Minimum Essential Medium (cat. No. 10–009-CV, Corning, New York, NY, USA) supplemented with 10% Fetal Bovine Serum (FBS, cat. No. 35–079-CV, Corning) and 1% Penicillin-Streptomycin Solution (P/S, cat. No. 30–002-CI, Corning). MDA-MB-231 cells were cultured in Dulbecco's Modified Eagle Medium (cat. No. 12–604F, Lonza, Basel, Switzerland) supplemented with 10% FBS and 1% P/S. Cells were maintained up to the fifth passage. Cellular morphology and confluence were monitored on an Olympus CKX53 inverted light microscope (Evident Microscopy Technologies, Shinjuku-ku, Tokyo, Japan). Routine checks for Mycoplasma contamination were conducted by staining with 4',6-Diamidino-2-phenylindole dihydrochloride (cat. No. D9542, Merck KGaA, Darmstadt, Germany).

Cell Transfection

To reduce MYO6 expression, a mixture consisting of 82 µL of SE Cell Line Nucleofector™ Solution, 12 µL of Supplement 1 reagent (Amaxa, SE Cell Line 4D-Nucleofector X Kit L, cat. No. V4XC-1024, Lonza, Basel, Switzerland), and 5 µL of a 10 µM siRNA solution (cat. No. sc-37133, Santa Cruz Biotechnology, Dallas, TX, USA) was used to suspend 1.5 million cells. Cuvettes containing the cell mixture were placed into the 4D-Nucleofector™ device (Lonza). The CH-125 pulse program was used for MDA-MB-231 cells, and the EN-130 pulse program was used for MCF-7 cells. The transfected cells were then transferred to culture vessels. After 24 h, the culture medium was replaced. Transfection efficiency was evaluated by examining fluorescence of cells after introducing the pmaxGFP plasmid included in the transfection kit, using the Tali® Image-based cytometer (Invitrogen Life Technologies, Carlsbad, CA, USA). Non-transfected cells (incubated with transfection buffer and electroporated with the appropriate program) and cells transfected with siRNA with a sequence that does not target human mRNA (cat. No. sc-37007, Santa Cruz Biotechnology) were used as controls. All assays were performed 72 hours after transfection.

Immunoblotting

Cells were centrifuged for 2 minutes at 1200 rpm, 4°C, washed with cold phosphate buffered saline (PBS), and centrifuged again. Cell pellets were stored at −80 °C. Cell pellets were suspended in a lysis buffer containing 50 mm Tris (pH 8.0), 120 mm NaCl, 0.5% NP-40 with protease (cat. No. 78438, Thermo Fisher Scientific, Waltham, MA, USA) and phosphatase inhibitors (cat. No. 78426, Thermo Fisher Scientific). Cell lysis was carried out on ice for 15 min. The samples were then centrifuged (14,000 rpm, 20 min, 4 °C), and the supernatants were transferred to clean Eppendorf tubes. Loading buffer consisting of 150 mm Tris (pH 6.8), 6% SDS, 30% glycerol, 0.01% bromophenol blue, and 7.5% β-mercaptoethanol (volume equal to half the volume of the lysate) was added. The lysates were incubated at 95 °C for 5 min and then stored at −80 °C. Samples were loaded onto a 10–20% Tris-Glycine Gel polyacrylamide gel (Novex™ WedgeWell™ Thermo Fisher Scientific), electrophoresed, and transferred to a nitrocellulose membrane (iBlot®2 NC Regular Stacks, Invitrogen Life Technologies) with an iBlot™ 2 Dry Blotting System (Invitrogen Life Technologies). The membranes were blocked with a 2.5% milk solution in PBS-Tween (PBST) for 1 h at room temperature (RT), incubated overnight at 4 °C with primary antibodies (Table 1), washed in PBST, and incubated with appropriate secondary antibodies (Table 2) for 1 hour at RT. The membranes were washed in PBST, and signal was detected with SuperSignal™ West Pico PLUS Chemiluminescent Substrate (cat. No. 34578, Thermo Fisher Scientific). Images were captured with the ChemiDoc MP Imaging System (Bio-Rad, Hercules, CA, USA), and band intensity was measured with ImageLab software (Bio-Rad). Glyceraldehyde-3-phosphate Dehydrogenase was used as a reference protein.

Table 1 Primary Antibodies (IF – Immunofluorescence Labeling, WB – Western Blot)

Molecular target	Dilution	Host	Manufacturer	Cat. No.
GAPDH	1:1000 WB	Mouse	Santa Cruz Biotechnology	sc-47724
GIPC1	1:50 IF 1:3000 WB	Rabbit	Proteintech	14B22-1AP
MYO6	1:50 IF	Rabbit	Proteintech	26778-1-AP
MYO6	1:500 WB	Mouse	Santa Cruz Biotechnology	sc-393558
SEPT2	1:100 IF 1:3000 WB	Rabbit	Proteintech	11397-1-AP
SEPT7	1:100 IF 1:3000 WB	Rabbit	Proteintech	13818-1-AP

Table 2 Secondary Antibodies (HRP – Horseradish Peroxidase, IF – Immunofluorescence Labeling, WB – Western Blot)

Type	Dilution	Conjugated particle	Manufacturer	Cat. No.
Anti-mouse	1:200 IF	Alexa Fluor 594	ThermoFisher Scientific	A11005
Anti-rabbit	1:200 IF	Alexa Fluor 594		A21207
Anti-mouse	1:4000 WB	HRP		31430
Anti-rabbit	1:4000 WB	HRP		31460

Fluorescence Labeling of Proteins

Cells were seeded onto sterile 18 mm glass coverslips in 12-well plates after transfection. After 72 h, cells were fixed with 4% paraformaldehyde (PFA, cat. No. 28906, Thermo Fisher Scientific) for 20 min at RT, washed three times with PBS for 5 min at RT, permeabilized in 0.25% Triton X-100 in PBS for 10 min at RT, and incubated with PBS plus 4% bovine serum albumin (BSA, cat. No. 9048–46-8, Merck KGaA) for 1 h at RT. Subsequently, the cells were incubated with primary antibodies (Table 1) for 1 h at RT, washed, and incubated with appropriate secondary antibodies (Table 2) in PBS for 1 h at RT in the dark. Cells were stained with Alexa Fluor 488 phalloidin (cat. No. A12379, Invitrogen) diluted 1:20 in PBS for 20 min at RT in the dark and DAPI (diluted 1:100 in distilled water) for 10 min at RT in the dark. The coverslips were mounted with Aqua Poly/Mount (cat. No. 18606–5, Polysciences). Images were captured on a C1 confocal microscope (Nikon, Tokyo, Japan) with a 60× oil immersion objective and Nikon EZ-C1 software (Nikon). Laser power, gain, and pixel dwell time were kept constant for all replicates for each protein.

Wound-Healing Assay

Cells were cultured in 6-well plates for 72 h, reaching approximately 100% confluence. Next, a scratch was made in the center of each well with a sterile 100 µL pipette tip. The plates were then maintained on an inverted motorized microscope (Zeiss) equipped with an incubation system for live-cell imaging (Pecon), which included an EC Plan-Neofluar 10×/0.30 Ph1 air objective, Axiocam 503 mono camera, and ZEN 2 software. Images were captured every 10 min for 36 h. The wound area and other relevant parameters were measured with ImageJ software (NIH).

Transwell Migration Assay

Cell culture inserts with 8 µm pores (cat. No. 140620, Thermo Fisher Scientific) were placed in a 24-well plate. At 72 h post-transfection, cells were seeded onto the inserts at a density of 1×10^5 cells per well in culture medium supplemented with 1% FBS. Medium containing 20% FBS was added beneath the inserts. Then, the cells were cultured for 24 h at 37 °C, 5% CO_2, 95% humidity. Next, the transwells were fixed with a 4% PFA solution. The cells were permeabilized with 80% ice-cold methanol for 20 min at RT, then stained with a 0.1% methylrosaniline chloride solution (PPF-HASCO-LEK S.A, Wrocław, Poland) for 20 min at RT. Cells unable to migrate through the membrane pores were removed from the inner surface of the insert with cotton swabs. The outer surface of the insert membrane was photographed on a light microscope equipped with a CCD digital camera (DS-5Mc-U1), and cells were counted with ImageJ software.

Cell Adhesion Assay

Cells were cultured for 72 h after transfection and then detached and seeded at a density of 0.4×10^6 cells per well in a 6-well plate. After 0.5, 1, 1.5, 2, 4, 6, and 24 h, the cells were washed with warm PBS, and images of each well surface were captured at 5 randomly selected locations. The number of cells capable of adhering to the substrate were counted with ImageJ (NIH).

Open-Field Cell Migration

At 72 hours after transfection, cells were cultured in 12-well plates for 24 h. Then, the culture medium was replaced, and the plates were positioned in an inverted motorized microscope (Zeiss) equipped with a live-cell imaging incubation system (Pecon). The imaging setup used an EC Plan-Neofluar 10×/0.30 Ph1 air objective, Axiocam 503 mono camera, and ZEN 2 software. Cell images were captured from three randomly selected fields in each well. The Manual Tracking plugin for ImageJ (NIH) was used to analyze cell movement. The Chemotaxis and Migration Tool 2.0 (Ibidi) was used to quantify aspects of cell migration dynamics, including velocity, Euclidean distance, and accumulated distance.

Statistical Analysis

All experiments were conducted with a minimum of three independent replicates. GraphPad Prism version 8.0.1 for Windows (GraphPad Software, Boston, MA, USA) was used for statistical analyses. The distribution of the results obtained in each experiment was initially assessed using the Shapiro–Wilk normality test. Depending on the outcome, either parametric tests (in cases of normal distribution) or non-parametric tests (in other cases) were used to analyze the statistical significance of differences between groups. Non-parametric test used to evaluate differences between two groups was Mann–Whitney *U*-test (MYO6, GIPC1, SEPT2, and SEPT7 mRNA expression and open fields analysis). Both, Box and whiskers plot, and violin plot presented min to max range. Parametric tests included one-way ANOVA with multiple comparisons (Western blot analysis of MYO6 protein level, wound healing assay), unpaired *t*-test (Western blot analysis of SEPT2, SEPT7, and GIPC1 protein level) and two-way ANOVA (transwell migration, cell adhesion). Data are reported as mean ±standard deviation. To evaluate the homogeneity of cell movement, Chemotaxis and Migration Tool 2.0 (Ibidi), was used. Significance is denoted on figures as * P<0.05, ** P<0.01, *** P<0.001, or **** P<0.0001).

Results

MYO6, GIPC1, SEPT2, and SEPT7 are Overexpressed in Breast Cancer Patient Tissues

To assess the expression of MYO6, GIPC1, SEPT2, and SEPT7 and their clinical relevance in breast cancer, we performed an in silico analysis of mRNA abundance of MYO6, GIPC1, SEPT2, and SEPT7 in healthy and breast cancer tissues in The Cancer Genome Atlas (TCGA) and Genotype Tissue Expression (GTEx) databases. We found that mRNA for all four genes was higher in breast cancer tissue than in normal tissue (Figure 1A–D).

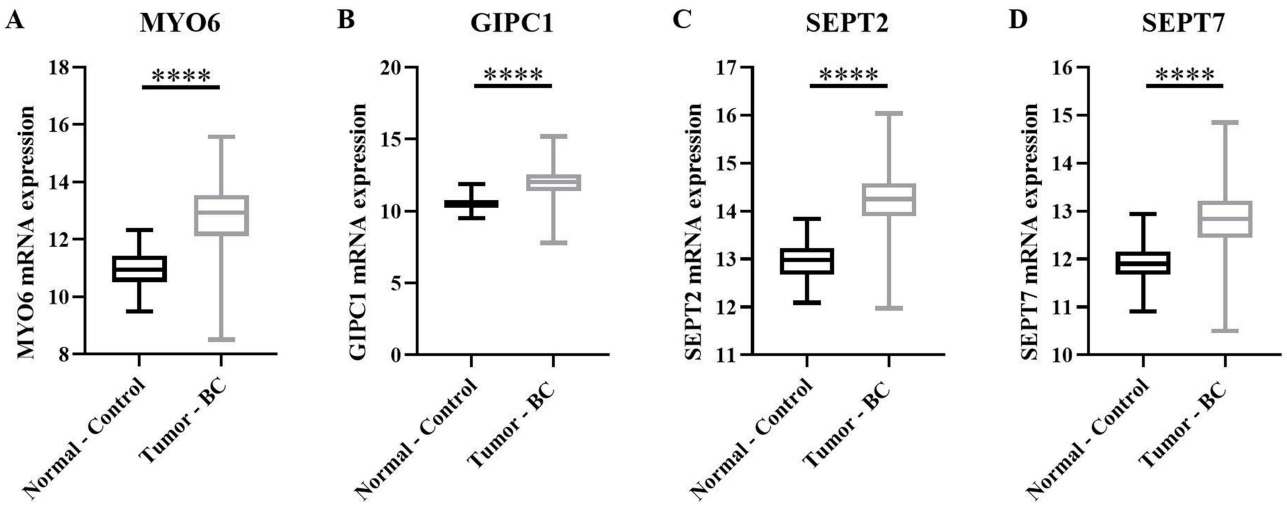

Figure 1 Expression of MYO6 (**A**), GIPC1 (**B**), SEPT2 (**C**), and SEPT7 (**D**) mRNA in normal tissue (Normal-Control) and breast cancer tissue (Tumor-BC). mRNA for all four genes are higher in breast cancer tissue than in normal tissue. Data is presented as median and IRQ with whiskers showing the whole value range. Data are from in silico analysis of The Cancer Genome Atlas and The Genotype-Tissue Expression databases. BC, breast cancer. ****P < 0.0001.

MYO6 is Required for Proper Cell Morphology and Expression of GIPC1, SEPT2, and SEPT7 in Breast Cancer Cells

To determine the extent to which MYO6 is required for expression and localization of GIPC1, SEPT2, and SEPT7 in breast cancer cells, we used siRNA to knock down MYO6 in MDA-MB-231 and MCF-7 cells. Transfection efficiency was estimated at 81.4% and 92.5% for MDA-MB-231 and MCF-7 cell lines, respectively (Figure 2A and B). The greatest decrease in MYO6 protein was evident at 72 hours after transfection in both cell lines (Figure 3A and B), so we used this time point in all experiments. Although MDA-MB-231 cells in which MYO6 was knocked down had normal morphology, MCF-7 cells in which MYO6 was knocked down were large, highly flattened, and multinucleated, suggesting they had undergone mitotic catastrophe (Figure 4).

We next examined the effect of MYO6 knock down on GIPC1, SEPT2, and SEPT7 by immunofluorescence. In non-transfected MDA-MB-231 cells, GIPC1 predominantly localized to cytoplasmic extensions at the cell periphery, but very little GIPC1 staining was evident in cells with reduced MYO6. In non-transfected MCF-7 cells, GIPC1 was concentrated in the cortical region of cells at the outermost part of the cluster. In MYO6 siRNA-transfected cells, GIPC1 expression was greatly reduced (Figure 5). MYO6 knockdown had little effect on SEPT2 expression in MDA-MB-231 cells. In non-transfected MCF-7 cells, SEPT2 was primarily localized along actin filaments and in the cortical regions of cells. In MCF-7 cells transfected with MYO6 siRNA, the SEPT2 fluorescence signal was notably weaker (Figure 6). Finally, in both non-transfected cell lines, SEPT7 fluorescence intensity was highest within the cytoplasmic extensions at the cell periphery and was also

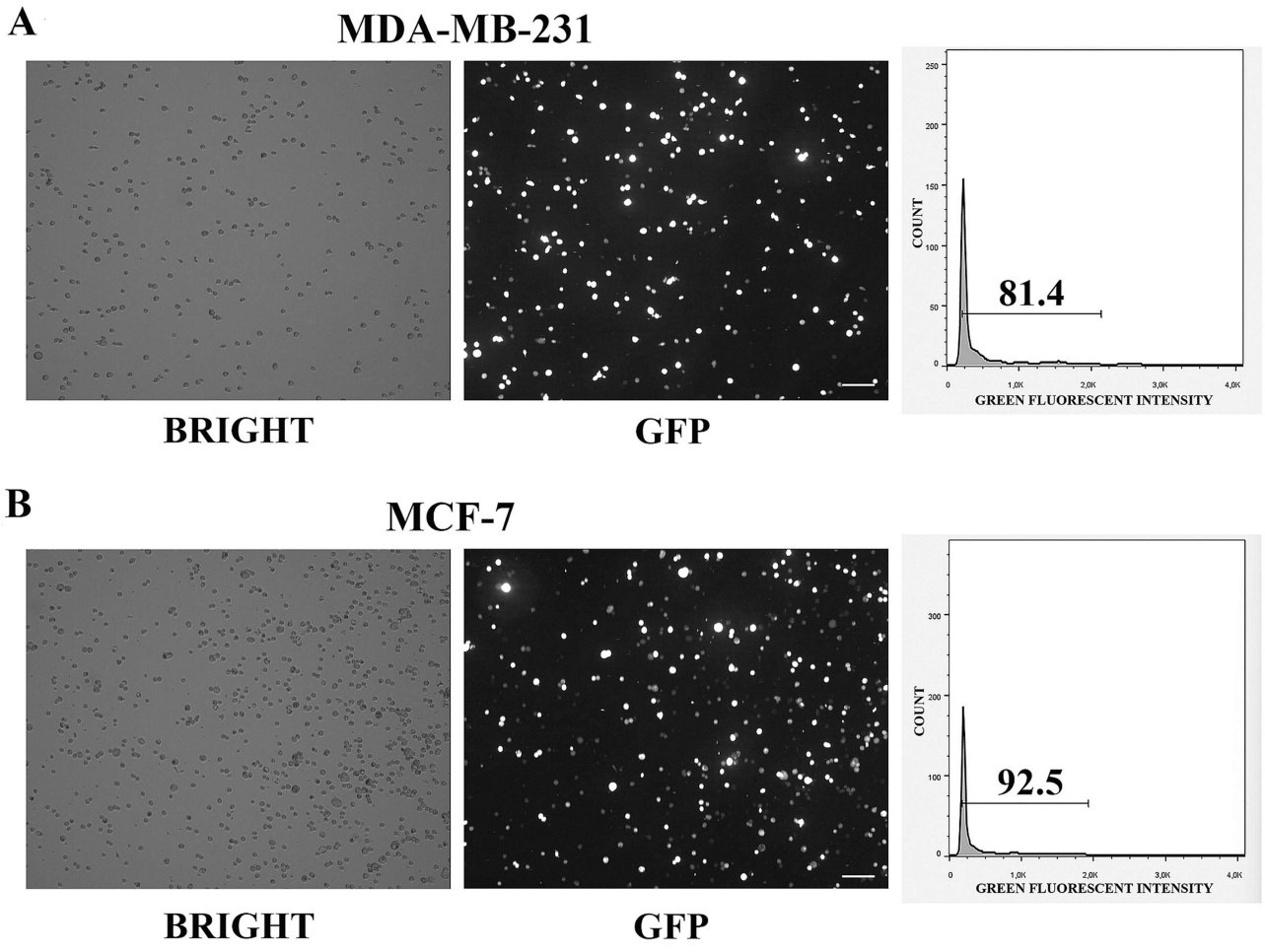

Figure 2 MYO6 siRNA transfection was efficient. Shown are representative bright-field images, green fluorescence protein GFP images, and quantitation of GFP in MDA-MB-231 (**A**), and MCF-7 (**B**) cell lines 72 h post-transfection. Transfection efficiency is estimated at 81.4% and 92.5% for MDA-MB-231 and MCF-7 cell lines, respectively. The experiment was repeated 3 times. Scale bar = 50 μm.

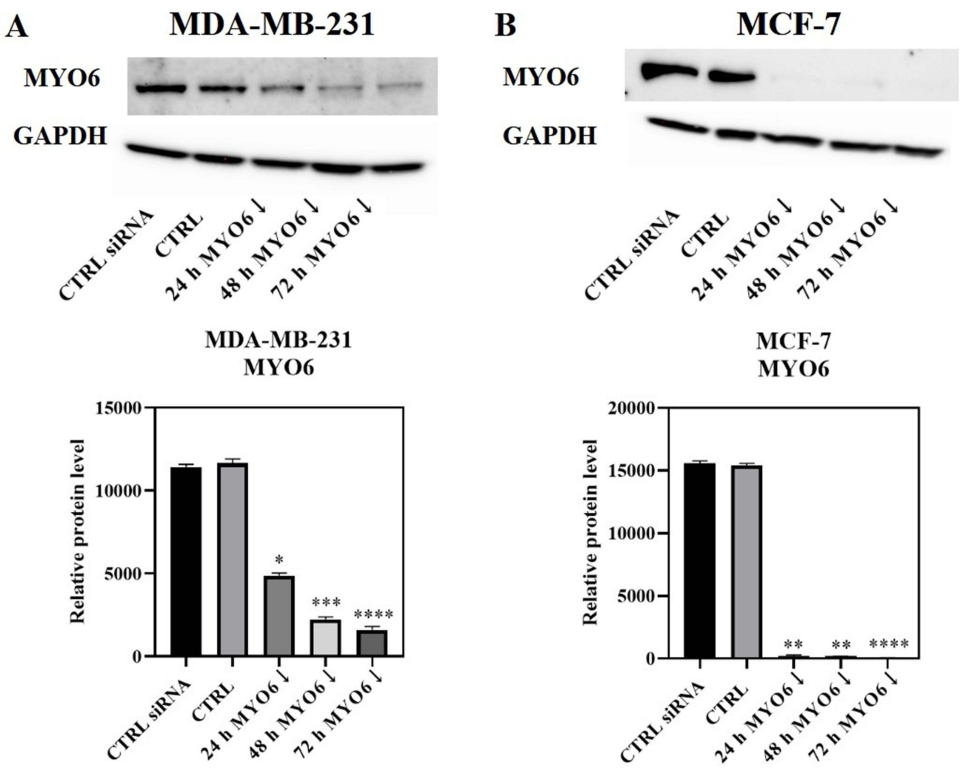

Figure 3 MYO6 siRNA substantially reduces MYO6 protein abundance. Shown are representative Western blots and quantitation of MYO6 in MDA-MB-231 (**A**), and MCF-7 (**B**) cell lines. The greatest decrease in MYO6 protein is evident at 72 hours after transfection in both cell lines Non-targeting siRNA – cells transfected with siRNA with a sequence that does not target human mRNA, Control – non-transfected cells, MYO6↓ - cells transfected with MYO6 siRNA. The experiment was repeated 6 times. *P< 0.05, **P < 0.01, ***P< 0.001, and ****P < 0.0001.

distributed along actin filaments. Conversely, in cells transfected with MYO6 siRNA, the visible fluorescence was significantly diminished and diffuse (Figure 7).

To confirm our immunofluorescence findings, we performed Western blots. In both MDA-MB-231 and MCF-7 cells, the abundances of GIPC1 and SEPT7 were both decreased in cells in which MYO6 was knocked down (Figure 8A and C). SEPT2 was slightly elevated in MDA-MB-231 cells in which MYO6 was knocked down and decreased in MCF-7 cells in which MYO6 was knocked down (Figure 8B). Together, these experiments suggest that MYO6 is required for proper cell morphology and expression of GIPC1, SEPT2, and SEPT7 in two breast cancer cell lines.

MYO6 Downregulation Impairs Migration of Breast Cancer Cells

We performed several in vitro assays to determine the impact of MYO6 downregulation on the migratory potential of MDA-MB-231 and MCF-7 cells. First, we performed the scratch wound-healing assay and found that MYO6 knock down significantly reduced migration of MDA-MB-231 cells (Figure 9A and B) but not of MCF-7 cells (Figure 9C and D). Second, we performed a transwell migration assay and found that MYO6 knock down significantly decreased migration of both MDA-MB-231 and MCF-7 cells by 3- and 1.8-fold, respectively (Figure 10A and B). Third, we assessed cell adhesive capacity of the MDA-MB-231 and MCF-7 cell lines and found that MYO6 knock down significantly decreased cell adhesion by an average of 1.9-fold at all but one time point assessed (Figure 11A and B). Finally, we examined cell migration behavior. In both MDA-MB-231 and MCF-7 cells, knock down of MYO6 decreased the accumulated distance traveled by the cells and their velocity (Figure 12A–C, Supplementary Videos S1, S2, S3, S4, S5, S6, S7, and S8).

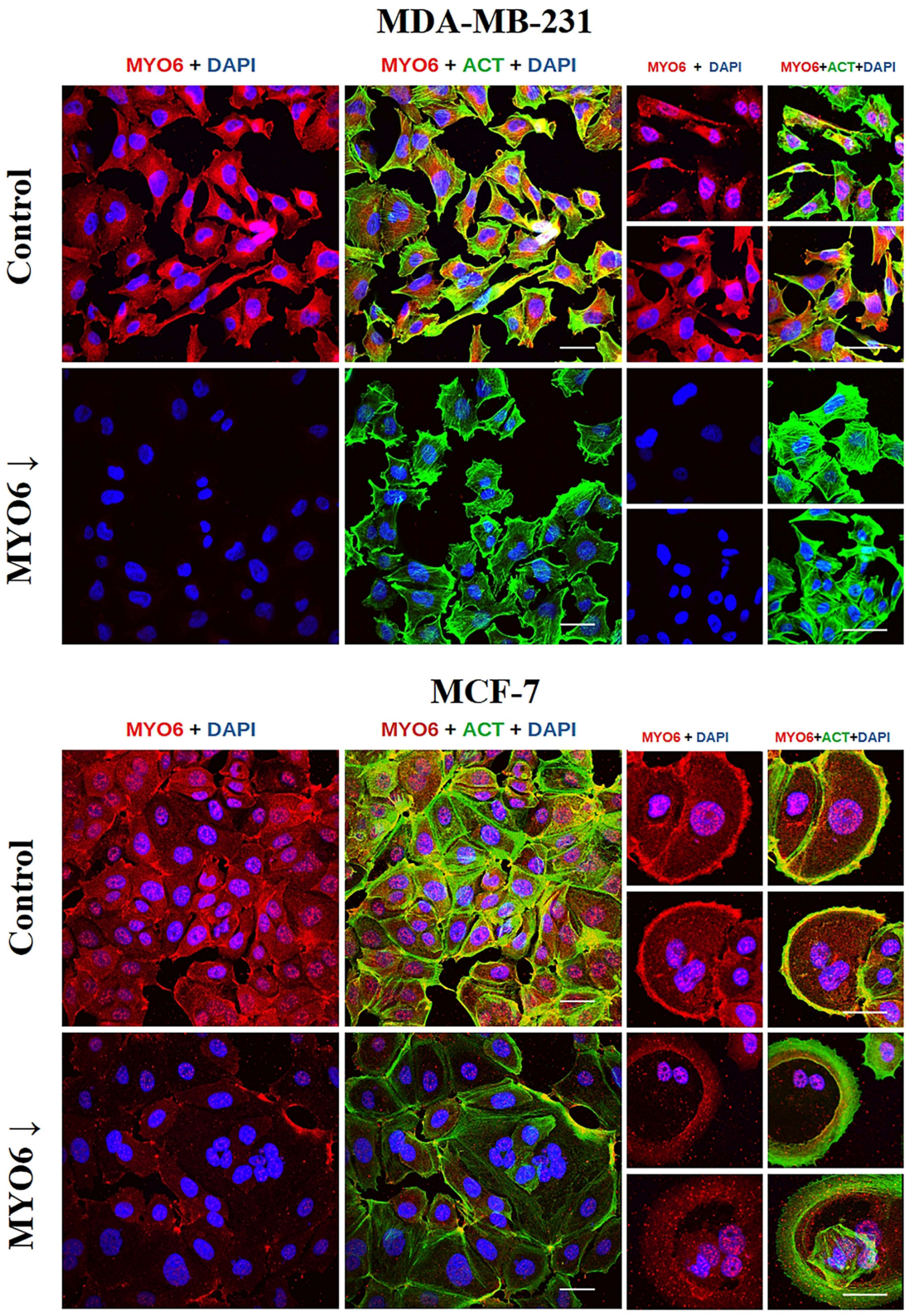

Figure 4 MYO6 siRNA reduces MYO6 protein expression in two breast cancer cell lines. Shown are representative fluorescent microscopy images of MYO6 (red), F-actin (ACT, green), and DAPI (blue) in the indicated cell lines. Control – non-transfected cells, MYO6↓ – cells transfected with MYO6 siRNA. The experiment was repeated 3 times. Scale bar = 50 μm.

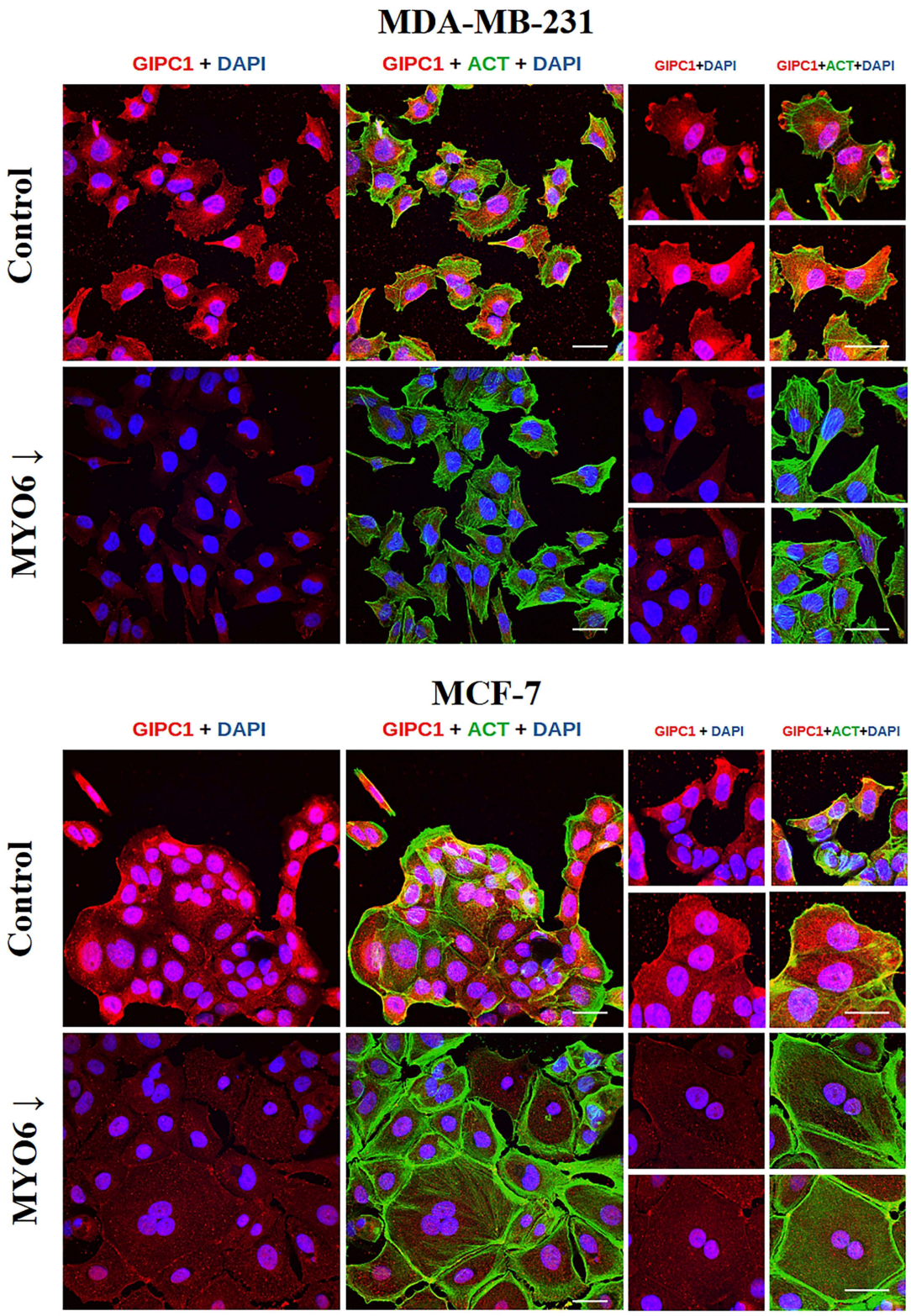

Figure 5 MYO6 siRNA reduces GIPC1 protein expression in two breast cancer cell lines. Shown are representative fluorescent microscopy images of GIPC1 (red), F-actin (ACT, green), and DAPI (blue) in the indicated cell lines. Control – non-transfected cells, MYO6↓ – cells transfected with MYO6 siRNA. The experiment was repeated 3 times. Scale bar = 50 μm.

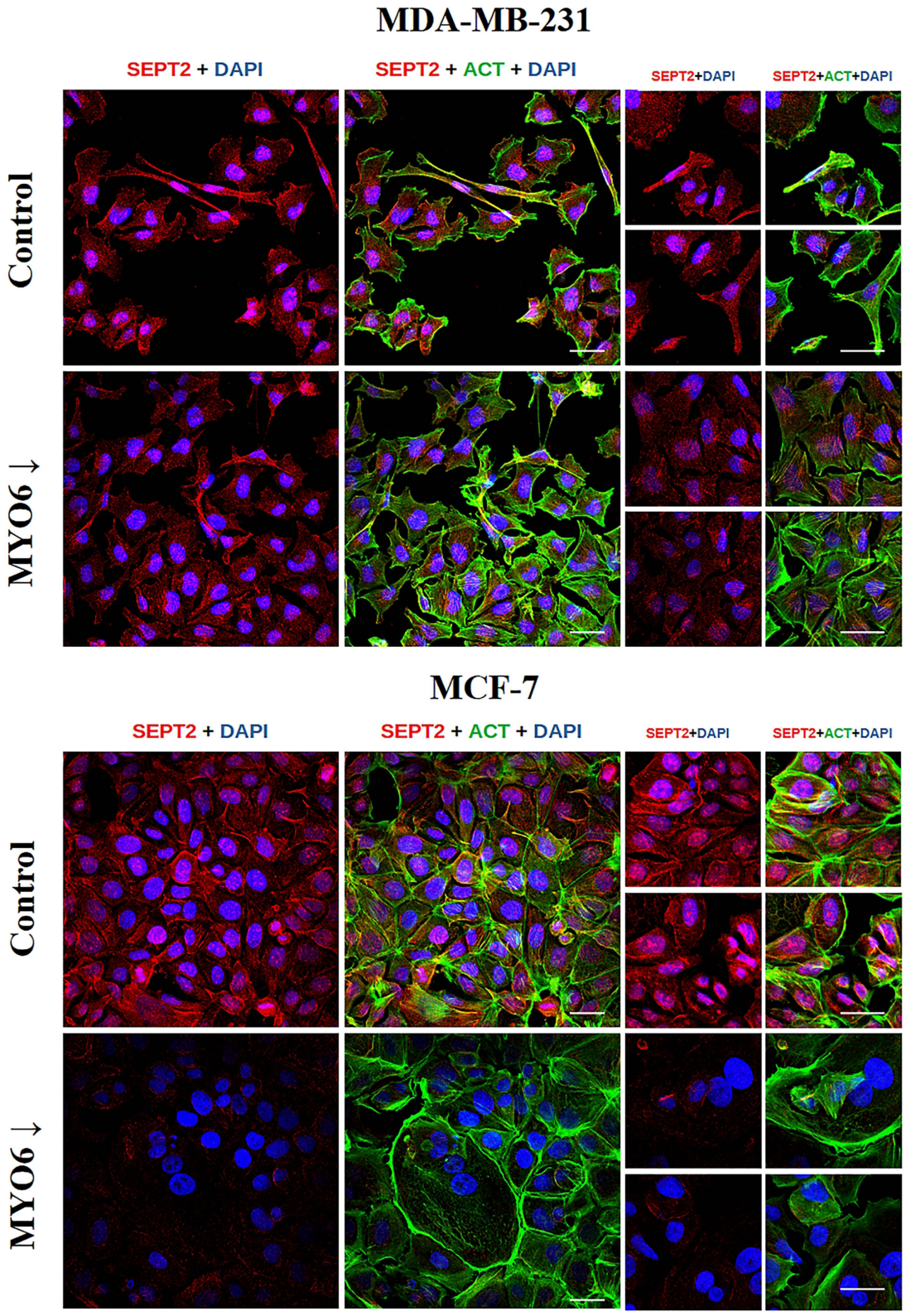

Figure 6 MYO6 siRNA reduces SEPT2 protein expression in two breast cancer cell lines. Shown are representative fluorescent microscopy images of SEPT2 (red), F-actin (ACT, green), and DAPI (blue) in the indicated cell lines. Control – non-transfected cells, MYO6↓ – cells transfected with MYO6 siRNA. The experiment was repeated 3 times. Scale bar = 50 μm.

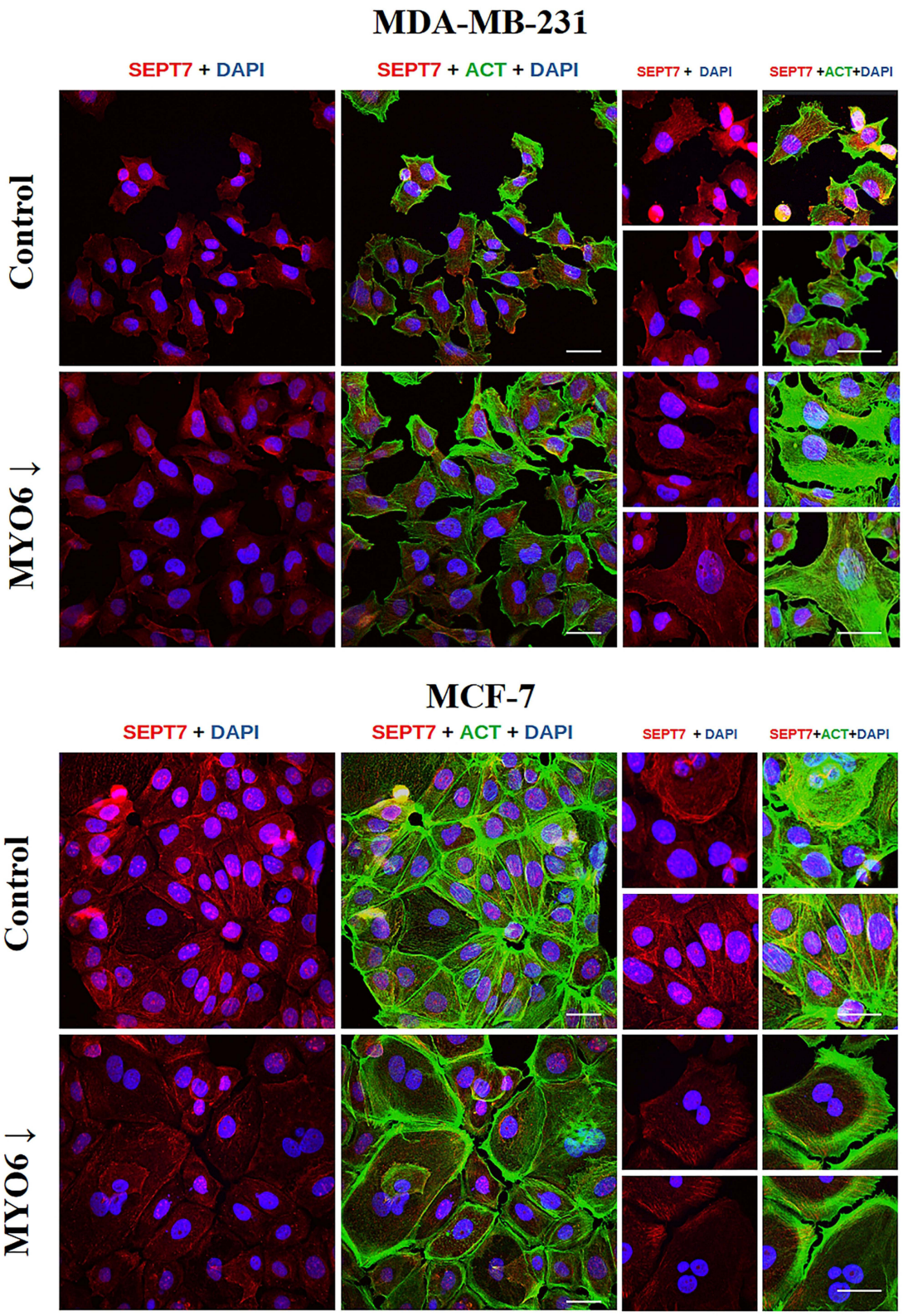

Figure 7 MYO6 siRNA reduces SEPT7 protein expression in MCF7 cells. Shown are representative fluorescent microscopy images of SEPT7 (red), F-actin (ACT, green), and DAPI (blue) in the indicated cell lines. Control – non-transfected cells, MYO6↓ – cells transfected with MYO6 siRNA. The experiment was repeated 3 times. Scale bar = 50 μm.

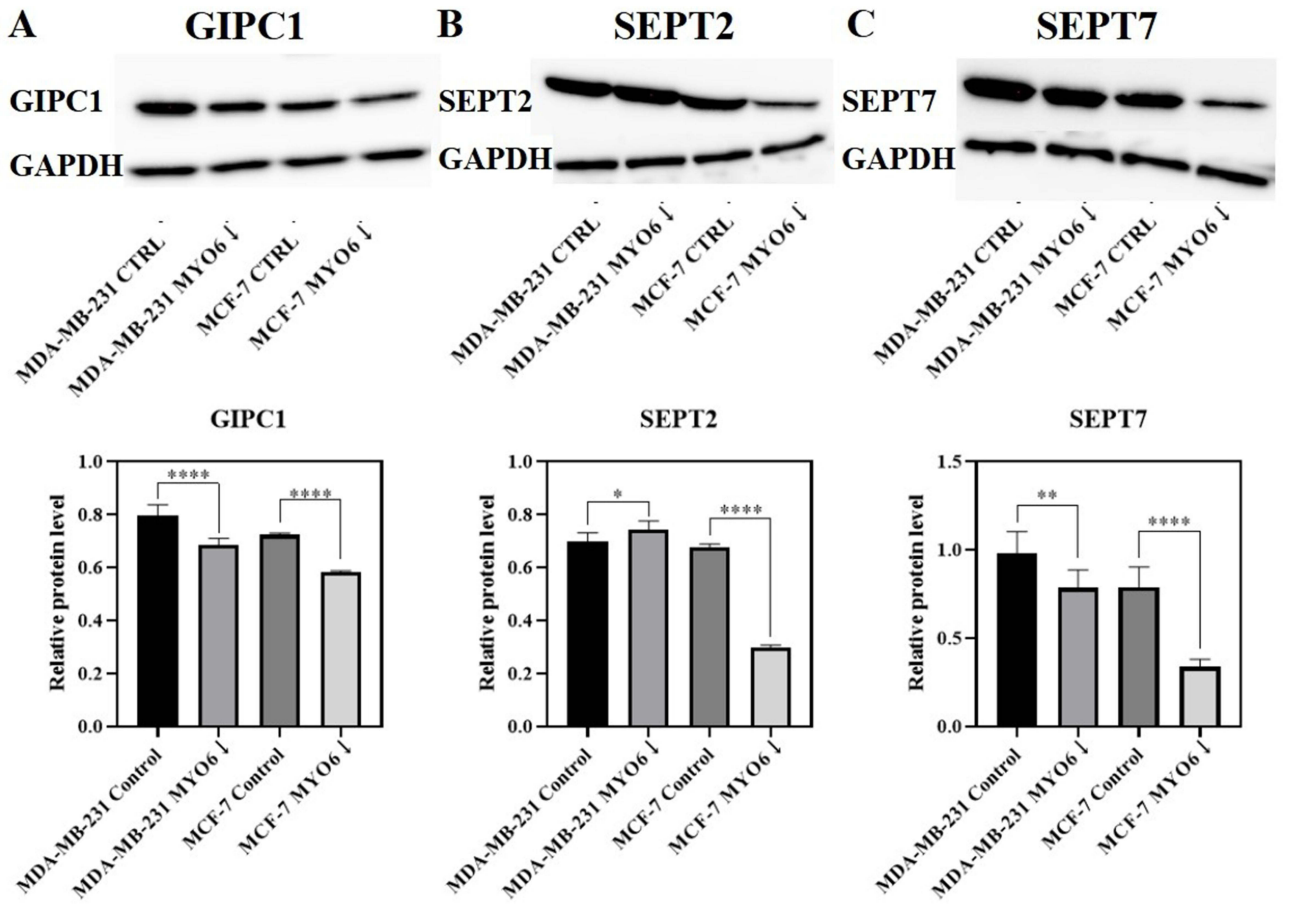

Figure 8 MYO6 siRNA decreases GIPC1 and SEPT7 expression breast cancer cell lines. Shown are representative Western blots and quantitation of (**A**) GIPC1, (**B**) SEPT2, (**C**) SEPT7 in the indicated cell lines. In both MDA-MB-231 and MCF-7 cells, the abundances of GIPC1 and SEPT7 are both decreased in cells in which MYO6 is knocked down. SEPT2 is slightly elevated in MDA-MB-231 cells in which MYO6 is knocked down and decreased in MCF-7 cells in which MYO6 is knocked down. Control – non-transfected cells, MYO6↓ - cells transfected with MYO6 siRNA. SEPT2 – Septin 2, SEPT7 – Septin 7. The experiment was repeated 6 times. *$P < 0.05$, **$P < 0.01$, ****$P < 0.0001$.

Discussion

Together, our data indicate that MYO6 contributes significantly to migratory abilities and regulates expression of GIPC, SEPT2, and SEPT7 in two breast cancer cell lines. First, we show that knock down of MYO6 alters the morphology of MCF-7 cells and reduces the expression of GIPC1 and SEPT7 in both MCF-7 and MDA-MB-231 cells. Second, in in silico data, we show that GIPC1, SEPT2, and SEPT7 are all overexpressed in breast cancer tissue samples from patients. Finally, we report that MYO6 knock down impairs migration and adhesion in both MCF-7 and MDA-MB-231 cells.

Our in silico data are consistent with data from Zhan et al (2023), who found that MYO6 expression was elevated in breast cancer cell lines (MDA-MB-231, MCF-7, T47D, and SKBR3) and tissues. They also found a correlation between high expression of this protein and poor prognosis for patients. Moreover, Zhan et al reported that MYO6 downregulation reduced proliferation, migration, and invasion of breast cancer cells.[3] These authors propose a potential role for MYO6 in promoting breast cancer cell migration through the MAPK/ERK pathway, suggesting it as a potential therapeutic target. These observations are consistent with the results of our current study, as we confirmed that downregulation of MYO6 in MCF-7 and MDA-MB-231 cell lines reduces their migratory abilities. However, both lines do not respond identically to MYO6 downregulation. For example, the assessment of cell migration using the wound-healing method showed that MYO6 knock down significantly reduced migration of MDA-MB-231 cells but not of MCF-7 cells. This is probably due to differences in the two cell line models -MCF7 positive—ER and PR, while MDA-MB-231 are triple negative.

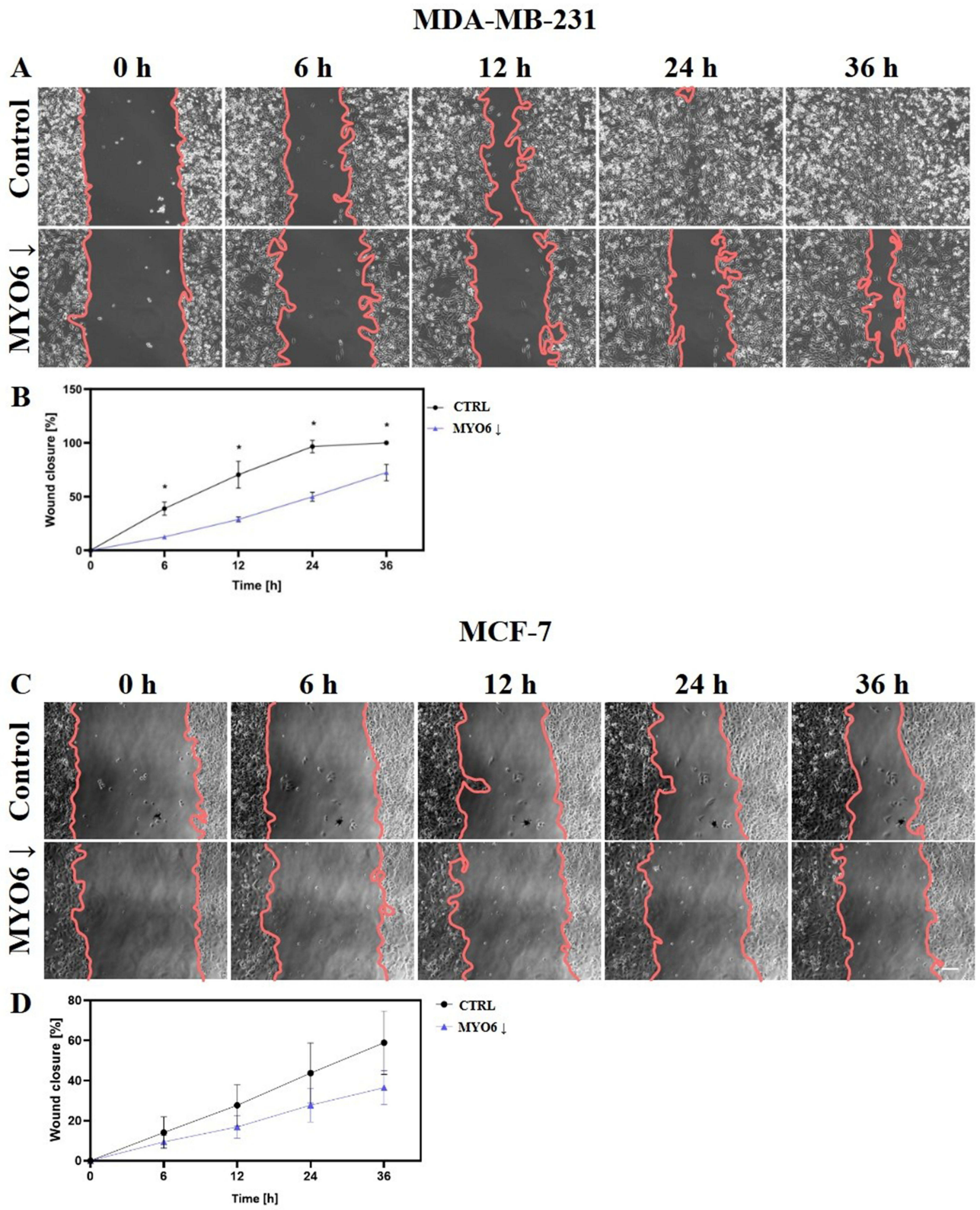

Figure 9 MYO6 siRNA reduces MDA-MB-231 cell migration in a wound-healing assay. Shown are (**A, C**) representative images of cells at indicated times after the scratch and (**B, D**) quantitation in (**A, B**) MDA-MB-231 and (**C, D**) MCF-7 cells. MYO6 knock down significantly reduce migration of MDA-MB-231 cells but not of MCF-7 cells. Control – non-transfected cells, MYO6↓ – cells transfected with MYO6 siRNA. The experiment was repeated 3 times. Scale bar = 50 μm. *$P < 0.05$.

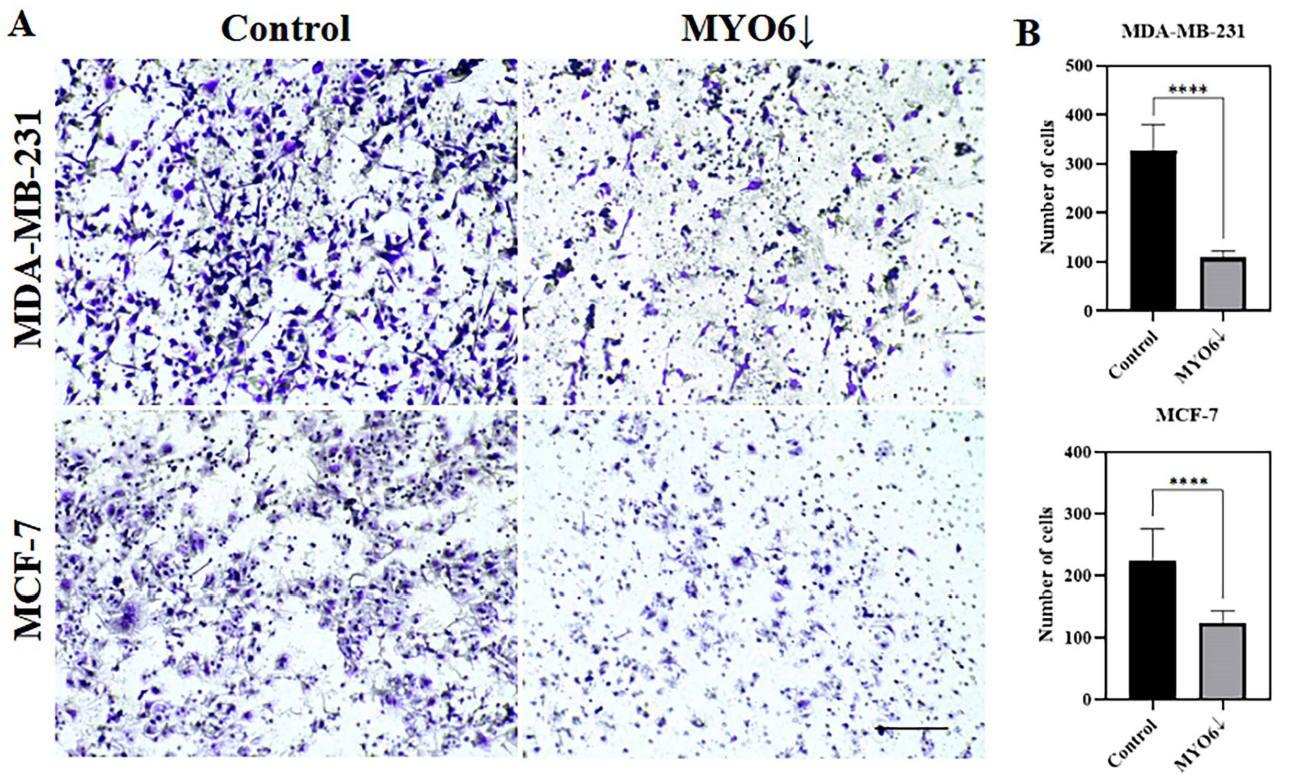

Figure 10 MYO6 siRNA reduces MDA-MB-231 and MCF-7 cell migration in a transwell migration assay. Shown are (**A**) representative images of the surface of the inserts and (**B**) quantitation of numbers of cells that were able to migrate through the 8 µm diameter insert pores in the indicated cell lines. MYO6 knock down significantly decrease migration of both MDA-MB-231 and MCF-7 cells. Control – non-transfected cells, MYO6↓ - cells transfected with MYO6 siRNA. The experiment was repeated 3 times. Scale bar = 100 µm.****$P < 0.0001$.

Our data regarding the effects of MYO6 knock down on expression of GIPC1 and SEPT7 in MCF-7 and MDA-MB-231 cells are consistent with previous observations in MCF-7 cells.[13] In our study, knock down of MYO6 reduced SEPT2 expression in MCF-7 cells but not in MDA-MB-231 cells. This difference may reflect inherent differences in these two breast cancer cell types. In Western blot analysis we observed higher expression of both SEPT2 and SEPT7 in MDA-MB-231 cells, which are more aggressive than MCF-7 cells. It is known that both cell lines differ in heterogeneity and genetic profile, hence probably a different response to the level of analyzed proteins.

We also noted that MYO6 knock down substantially altered MCF-7 cell morphology. Under standard conditions, these small cells typically formed compact clusters. However, after MYO6 downregulation, these cells increased in size, became flatter, grew as a monolayer, and frequently became multinucleated. This response may be due to the effects of SEPT2 expression, as Spiliotis et al suggested that SEPT2 plays a role in forming a scaffold at the midplane of the mitotic spindle, coordinating critical steps in mammalian mitosis.[19] Other reports have confirmed that inhibiting SEPT2 with antibodies resulted in multinucleation of cells.[20] Conversely, knock down of MYO6 did not reduce SEPT2 expression in or alter the morphology of MDA-MB-231 cells.

The functioning of MYO6, GIPC1 and SEPTs is closely related. Study by Katoh (2013) showed that GIPC1 interacts with the integrin α5 subunit, which pairs with the integrin β subunit to form integrin heterodimers. The GIPC1–MYO6 complex is responsible for the recycling of these heterodimers back to the plasma membrane. Integrins serve as mechano-sensory receptors that link the extracellular matrix to cytoplasmic adaptor proteins associated with actin filaments, making their recycling crucial for regulating actin dynamics. Specifically, GIPC1 is essential for the trafficking of internalized integrins, a process pivotal to cell migration, angiogenesis, and cytokinesis.[9] This is consistent with observations from our studies, where downregulation of MYO6 led to a decrease in GIPC1 protein levels and, concurrently, reduced the migratory capabilities of cells. O'Loughlin

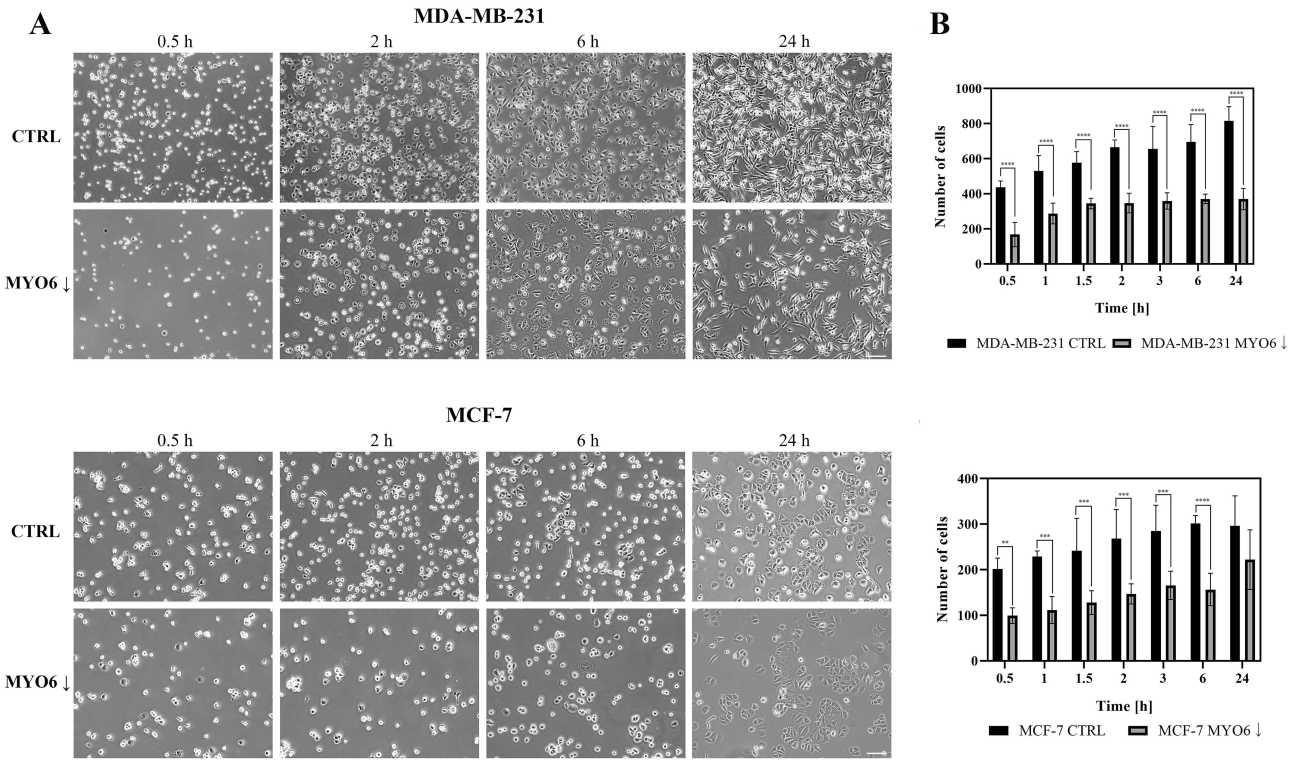

Figure 11 MYO6 siRNA reduces MDA-MB-231 and MCF-7 cell adhesion. Shown are (**A**) representative images of the cell monolayer and (**B**) quantitation of the numbers of cells able to adhere to the substrate in the indicated cell lines. MYO6 knock down significantly decrease cell adhesion by an average of 1.9-fold at all but one time point assessed in MDA-MB-231, and MCF-7 cell lines. Control – non-transfected cells, MYO6↓ - cells transfected with MYO6 siRNA. The experiment was repeated 3 times. Scale bar = 50 μm. $^{**}P < 0.01$, $^{***}P < 0.001$, $^{****}P < 0.0001$.

et al (2018) highlighted the critical role of the MYO6-GIPC1 complex in cell migration by demonstrating its involvement in filopodia formation. Additionally, they suggested a connection between MYO6 and the positioning of SEPT filaments.[15] MYO6 and SEPT2/7 stay in close relationship with each other as they all impact Ras-Raf-MEK-ERK signaling network, proved to regulate cell motility, invasiveness, and apoptosis.[21] Studies by Wang et al (2016) show that MYO6 knockdown reduces ERK1/2 phosphorylation in prostate cancer cells. From their experiments, the authors concluded that ERK1/2 is a downstream target of MYO6, and that the Ras-Raf-MEK-ERK pathway may be inhibited by MYO6 knockdown.[5] Similarly, Zhang et al (2016) observed that in SEPT7/2-depleted MDA-MB-231 breast cancer cells, both cell migration and invasion were significantly reduced compared to controls. They also demonstrated that MEK/ERK activation positively correlated with the protein levels of SEPT2 and SEPT7.[13] These findings suggest a functional link between MYO6 and SEPTs generally, and specifically with SEPT2 and SEPT7, via the MEK-ERK pathway. Our research supports this conclusions, as we also observed correlations between the protein levels of MYO6, SEPT2, and SEPT7 in breast cancer cells.

Conclusion

Based on our findings, MYO6 plays a crucial role in maintaining proper cell morphology and regulating the expression and localization of GIPC1, SEPT2, and SEPT7 in breast cancer cells. The downregulation of MYO6 impairs the migratory potential of these cells, as evidenced by reduced migration, adhesion, and movement velocity in both MDA-MB-231 and MCF-7 cell lines. However, there were notable differences in the response to MYO6 knockdown between the two cell lines. In MYO6 siRNA-transfected MCF-7 cells, a significant percentage exhibited altered morphology, while no such changes were observed in MDA-MB-231 cells. Additionally, MYO6 knockdown affected SEPT2 expression differently, causing an increase in MDA-MB-231 cells and a decrease in MCF-7 cells. This suggests that, despite similar outcomes, the underlying cellular mechanisms

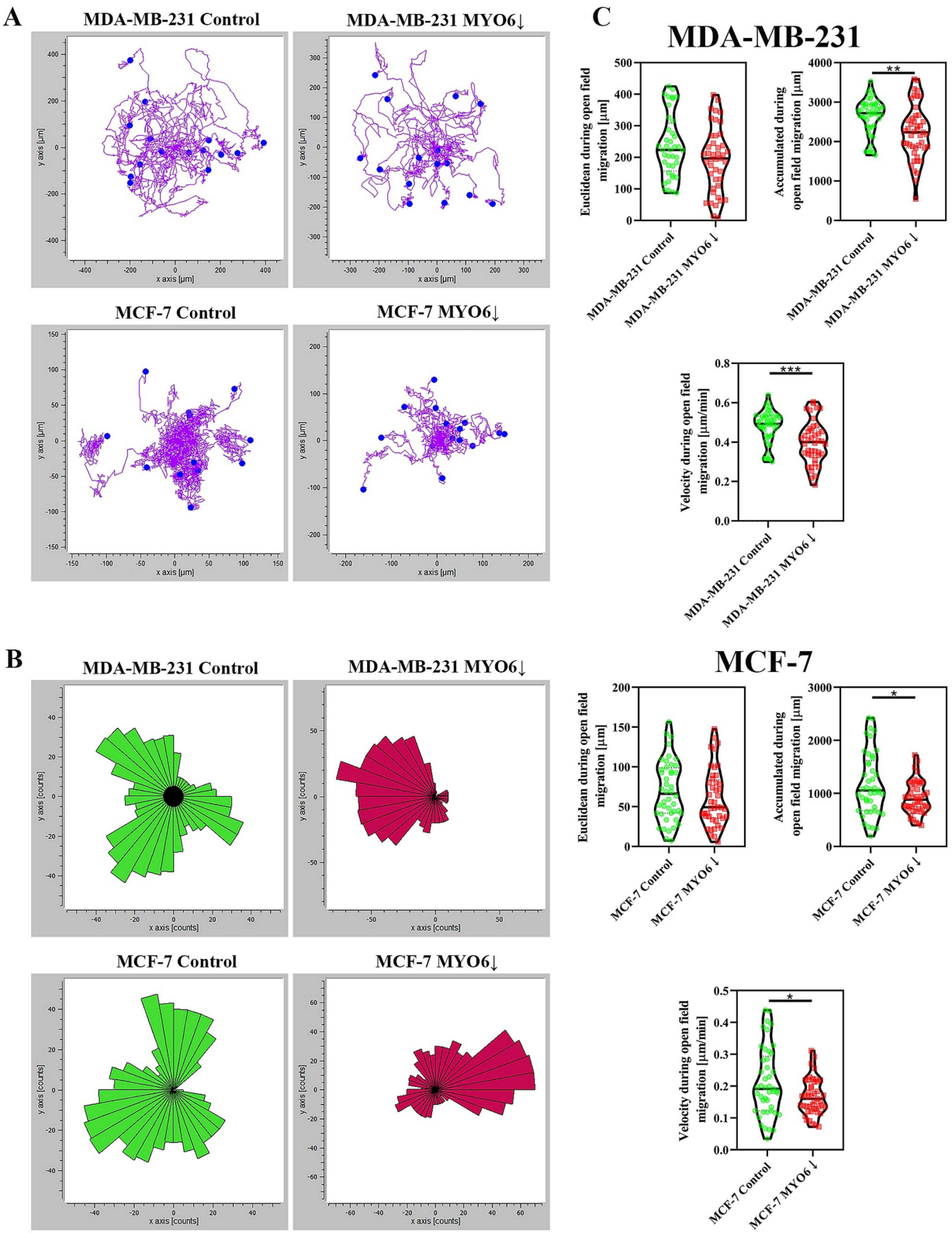

Figure 12 MYO6 siRNA reduces MDA-MB-231 and MCF-7 cell open field migration. Shown are (**A**) cell paths, (**B**) – rose plot presenting direction bias, (**C**) Euclidean distance (µm), accumulated distance (µm) and velocity (µm/min) for MDA-MB-231 and MCF-7 cells. The experiment was repeated 3 times. *$P < 0.05$, **$P < 0.01$, ***$P < 0.001$.

may vary depending on factors such as progesterone and estrogen receptor expression. These results indicate that MYO6 is essential for the migratory behavior of breast cancer cells and may be a potential target for therapeutic intervention. However, further studies are needed to fully elucidate the mechanism of action.

Ethics Approval and Informed Consent

Consent of the bioethics committee of Collegium Medicum UMK KB 477/2023

Patient consent for publication: Not applicable

The author(s) report no conflicts of interest in this work

Author Contributions

All authors made a significant contribution to the work reported, whether that is in the conception, study design, execution, acquisition of data, analysis or interpretation; took part in drafting, revising or critically reviewing the article and gave final approval of the version to be published. All authors have agreed on the journal to which the article has been submitted; and agree to be accountable for all aspects of the work.

Funding

The project was supported by a grant IDUB/IDE/2020 HS (to M.L.) from the Nicolaus Copernicus University in Toruń (Torun, Poland), the "Excellence Initiative – Research University – Inter Disciplinas Excellentia" programme. RL, MI, WA, and ML are members of the Emerging Field "Cells as EXperimental platforms and bioFACTories (CExFact)" - The "Excellence Initiative – Research University" programme.

Disclosure

The authors declare that the research was conducted in the absence of any commercial or financial relationships that could be construed as a potential conflict of interest.

References

1. Dillekås H, Rogers MS, Straume O. Are 90% of deaths from cancer caused by metastases? *Cancer Med*. 2019;8(12):5574–5576. doi:10.1002/cam4.2474
2. Masters TA, Buss F. Filopodia formation and endosome clustering induced by mutant plus-end-directed myosin VI. *Proc Natl Acad Sci U S A*. 2017;114(7):1595–1600. doi:10.1073/pnas.1616941114
3. Zhan XJ, Wang R, Kuang XR, Zhou JY, Hu XL. Elevated expression of myosin VI contributes to breast cancer progression via MAPK/ERK signaling pathway. *Cell. Signalling*. 2023;106:110633. doi:10.1016/j.cellsig.2023.110633
4. You W, Tan G, Sheng N, et al. Downregulation of myosin VI reduced cell growth and increased apoptosis in human colorectal cancer. *Acta Biochim Biophys Sin (Shanghai)*. 2018;50(7):731. doi:10.1093/abbs/gmy035
5. Wang D, Zhu L, Liao M, et al. MYO6 knockdown inhibits the growth and induces the apoptosis of prostate cancer cells by decreasing the phosphorylation of ERK1/2 and PRAS40. *Oncol Rep*. 2016;36(3):1285–1292. doi:10.3892/or.2016.4910
6. Meng W, Chen B, Jiang Z, Cai B, Ma L, Guan Y. A comprehensive analysis of MYO6 as a promising biomarker for diagnosis, prognosis, and immunity in clear cell renal cell carcinoma. *Transl Cancer Res*. 2023;12(8):2071–2098. doi:10.21037/tcr-23-227
7. Reed BC, Cefalu C, Bellaire BH, et al. GLUT1CBP(TIP2/GIPC1) Interactions with GLUT1 and Myosin VI: evidence supporting an adapter function for GLUT1CBP. *MBoC*. 2005;16(9):4183–4201. doi:10.1091/mbc.e04-11-0978
8. Rai A, Shrivastava R, Vang D, et al. Multimodal regulation of myosin VI ensemble transport by cargo adaptor protein GIPC. *J Biol Chem*. 2022;298(3):101688. doi:10.1016/j.jbc.2022.101688
9. Katoh M. Functional proteomics, human genetics and cancer biology of GIPC family members. *Exp Mol Med*. 2013;45(6):e26–e26. doi:10.1038/emm.2013.49
10. Rudchenko S, Scanlan M, Kalantarov G, et al. A human monoclonal autoantibody to breast cancer identifies the PDZ domain containing protein GIPC1 as a novel breast cancer-associated antigen. *BMC Cancer*. 2008;8(1):248. doi:10.1186/1471-2407-8-248
11. Yavelsky V, Rohkin S, Shaco-Levy R, et al. Native human autoantibodies targeting GIPC1 identify differential expression in malignant tumors of the breast and ovary. *BMC Cancer*. 2008;8(1):247. doi:10.1186/1471-2407-8-247
12. Wu D, Haruta A, Wei Q. GIPC1 interacts with MyoGEF and promotes MDA-MB-231 breast cancer cell invasion. *J Biol Chem*. 2010;285(37):28643–28650. doi:10.1074/jbc.M110.107649
13. Zhang N, Liu L, Fan N, et al. The requirement of SEPT2 and SEPT7 for migration and invasion in human breast cancer via MEK/ERK activation. *Oncotarget*. 2016;7(38):61587–61600. doi:10.18632/oncotarget.11402
14. Majewski Ł, Sobczak M, Havrylov S, Jóźwiak J, Rędowicz MJ. Dock7: a GEF for Rho-family GTPases and a novel myosin VI-binding partner in neuronal PC12 cells. *Biochem Cell Biol*. 2012;90(4):565–574. doi:10.1139/o2012-009
15. O'Loughlin T, Masters TA, Buss F. The MYO6 interactome reveals adaptor complexes coordinating early endosome and cytoskeletal dynamics. *EMBO Rep*. 2018;19(4):e44884. doi:10.15252/embr.201744884

16. Froidevaux-Klipfel L, Poirier F, Boursier C, et al. Modulation of septin and molecular motor recruitment in the microtubule environment of the Taxol-resistant human breast cancer cell line MDA-MB-231. *Proteomics*. 2011;11(19):3877–3886. doi:10.1002/pmic.201000789
17. Kinoshita M, Field CM, Coughlin ML, Straight AF, Mitchison TJ. Self- and actin-templated assembly of mammalian septins. *Dev. Cell*. 2002;3(6):791–802. doi:10.1016/S1534-5807(02)00366-0
18. Goldman MJ, Craft B, Hastie M, et al. Visualizing and interpreting cancer genomics data via the Xena platform. *Nat Biotechnol*. 2020;38(6):675–678. doi:10.1038/s41587-020-0546-8
19. Spiliotis ET, Kinoshita M, Nelson WJ. A mitotic septin scaffold required for mammalian chromosome congression and segregation. *Science*. 2005;307(5716):1781–1785. doi:10.1126/science.1106823
20. Kinoshita M, Kumar S, Mizoguchi A, et al. Nedd5, a mammalian septin, is a novel cytoskeletal component interacting with actin-based structures. *Genes Dev.* 1997;11(12):1535–1547. doi:10.1101/gad.11.12.1535
21. Song Y, Bi Z, Liu Y, Qin F, Wei Y, Wei X. Targeting RAS–RAF–MEK–ERK signaling pathway in human cancer: current status in clinical trials. *Genes Dis*. 2023;10(1):76–88. doi:10.1016/j.gendis.2022.05.006